Journal of Structural Geology 31 (2009) 1012–1027

Contents lists available at ScienceDirect

Journal of Structural Geology

journal homepage: www.elsevier.com/locate/jsg

The interplay of fold mechanisms and basement weaknesses at the transition between Laramide basement-involved arches, north-central Wyoming, USA

Thomas G. Neely*, Eric A. Erslev

Department of Geosciences, Colorado State University, Fort Collins, CO 80523, USA

ARTICLE INFO

Article history:
Received 25 April 2007
Received in revised form
17 September 2008
Accepted 12 March 2009
Available online 24 March 2009

Keywords:
Laramide
Basement-involved
Beartooth
Rattlesnake Mountain
Wyoming

ABSTRACT

Horizontally-shortened, basement-involved foreland orogens commonly exhibit anastomosing networks of bifurcating basement highs (here called arches) whose structural culminations are linked by complex transition zones of diversely-oriented faults and folds. The 3D geometry and kinematics of the southern Beartooth arch transition zone of north-central Wyoming were studied to understand the fold mechanisms and control on basement-involved arches.

Data from 1581 slickensided minor faults are consistent with a single regional shortening direction of 065°. Evidence for oblique-slip, vertical axis rotations and stress refraction at anomalously-oriented folds suggests formation over reactivated pre-existing weaknesses. Restorable cross-sections and 3D surfaces, constrained by surface, well, and seismic data, document blind, ENE-directed basement thrusting and associated thin-skinned backthrusting and folding along the Beartooth and Oregon Basin fault systems. Between these systems, the basement-cored Rattlesnake Mountain backthrust followed basement weaknesses and rotated a basement chip toward the basin before the ENE-directed Line Creek fault system broke through and connected the Beartooth and Oregon Basin fault systems. Slip was transferred at the terminations of the Rattlesnake Mountain fault block by pivoting to the north and tear faulting to the south. In summary, unidirectional Laramide compression and pre-existing basement weaknesses combined with fault-propagation and rotational fault-bend folding to create an irregular yet continuous basement arch transition.

1. Introduction

What controls the location and geometry of basement-involved deformation in foreland contractional orogens? Many foreland orogens, including the Sierras Pampeanas of western Argentina, the Tien Shan of central Asia, and the Laramide province of western North America (Fig. 1), record basement-involved shortening as irregular, roughly-spaced basement highs thousands of kilometers from plate boundaries. This paper refers to these basement highs as "arches", a more geometric term than "uplifts", which emphasizes vertical components of foreland deformation instead of the more important horizontal components of slip. These complex, anastomosing networks of bifurcating, elongate basement highs are defined by up-bowed pre-orogenic strata. Basement arches can be both symmetric and asymmetric, with widths of up to 100 km and lengths measured in hundreds of km (Fig. 1). Arch culminations are linked by complex transition zones between highs of differing orientations, vergences, and general geometries. These transition zones can be abrupt, gradual or transitional, and are commonly accompanied by secondary fault and fold structures.

Although early interpretations of Laramide structural geometries commonly relied on near-vertical, dip-slip faults to explain the region's irregular basement topography (Stearns, 1971), subsequent geophysical and kinematic studies documented horizontal shortening on arch-bounding thrust and reverse faults (Allmendinger and Jordan, 1983; Gries, 1983; Erslev, 2005). Still, the controls on the observed patterns of regional-scale foreland deformation remain contested, with current models calling on multi-stage, multi-directional shortening (Chapin and Cather, 1981; Gries, 1983; Bird, 1998), crustal buckling (Erslev, 1993, 2005), and lithospheric buckling (Tikoff and Maxson, 2001) or weakening (Humphreys et al., 2003) as well as local controls by pre-existing weaknesses (Brown, 1993; Marshak et al., 2000). And while the importance of fault-related folding is well recognized in these orogens, the relevance of thin-skinned fault-bend (Suppe, 1983), fault-propagation (Suppe and Medwedeff, 1990) and detachment (Epard and

* Corresponding author. Present address: Department of Geology and Geophysics, University of Wyoming, Laramie, WY, USA. Tel.: +1 281 293 4069; fax: +1 281 293 2548.
E-mail addresses: thomas.g.neely@conocophillips.com, eerslev@uwyo.edu (T.G. Neely).

0191-8141/$ – see front matter © 2009 Elsevier Ltd. All rights reserved.
doi:10.1016/j.jsg.2009.03.008

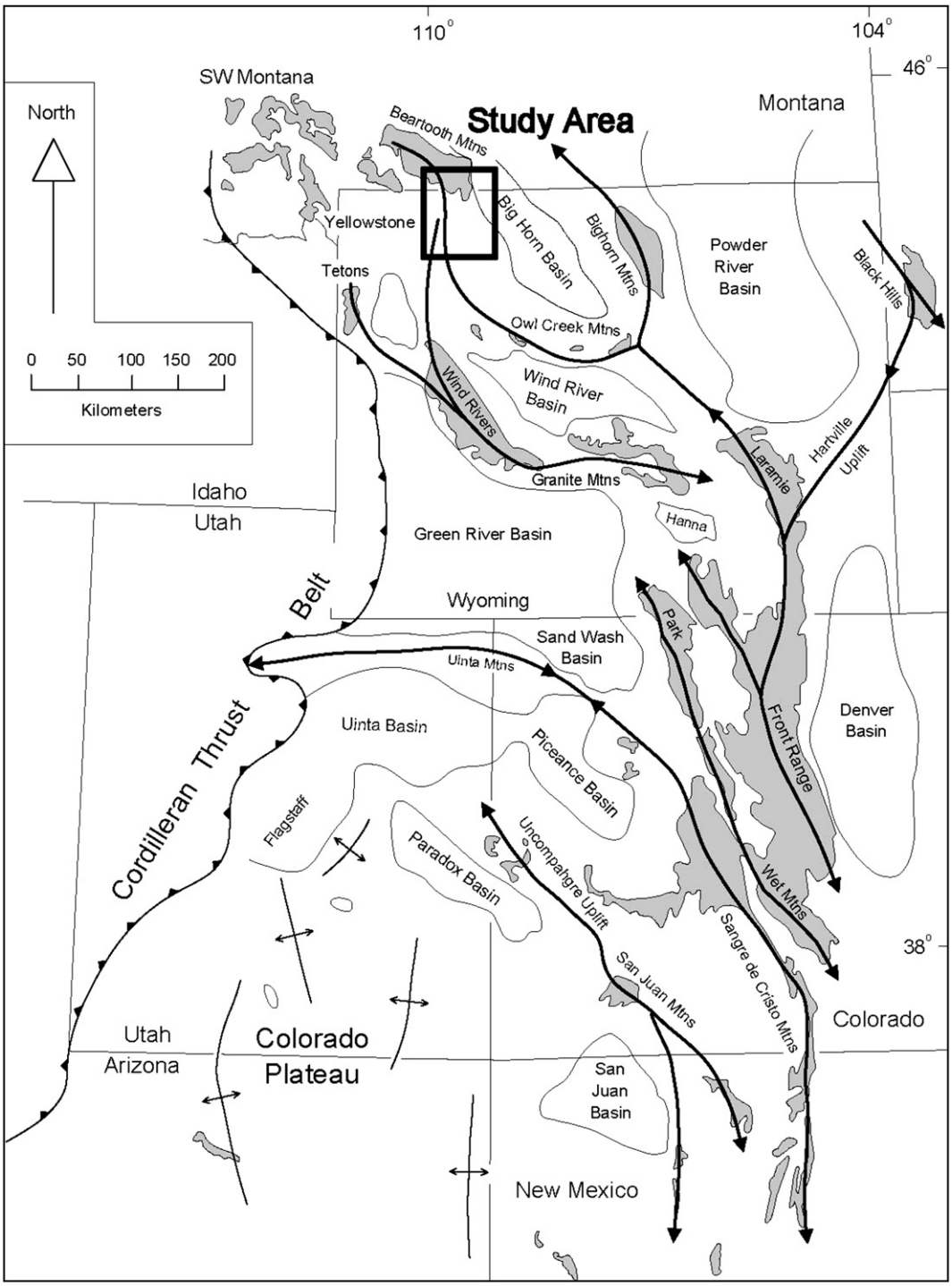

Fig. 1. Map showing exposures of Precambrian basement rocks (gray), Laramide basins (black outlines), principal Laramide arch trends (thick lines, arrows indicating arch plunge/termination), and study area location; from Erslev (2005).

Groshong, 1995) fold models has been challenged (Erslev, 1986, 1991; Allmendinger, 1998; Erslev and Hennings, 2004) due to the mechanical contrasts between layered sedimentary strata and underlying crystalline basement.

The diverse structural orientations at transitions between basement-involved foreland arches provide excellent tests of basement-involved deformation hypotheses. This study analyzes the 3D geometric and kinematic development of a Laramide (~70 to 55 Ma) arch transition zone in the Rocky Mountains of north-central Wyoming in order to understand the controls on arch development in basement-involved foreland orogens. We focused on the jog between the WNW-trending Beartooth arch and the NW-trending arch associated with the basin-bounding Line Creek and Oregon Basin fault systems of the northwestern Bighorn Basin (Figs. 1 and 2). The area contains excellent surface exposures and extensive subsurface petroleum industry data delineating a diverse array of basement-involved structures, which range from primary basin-boundary faults (Beartooth, Line Creek and Oregon Basin

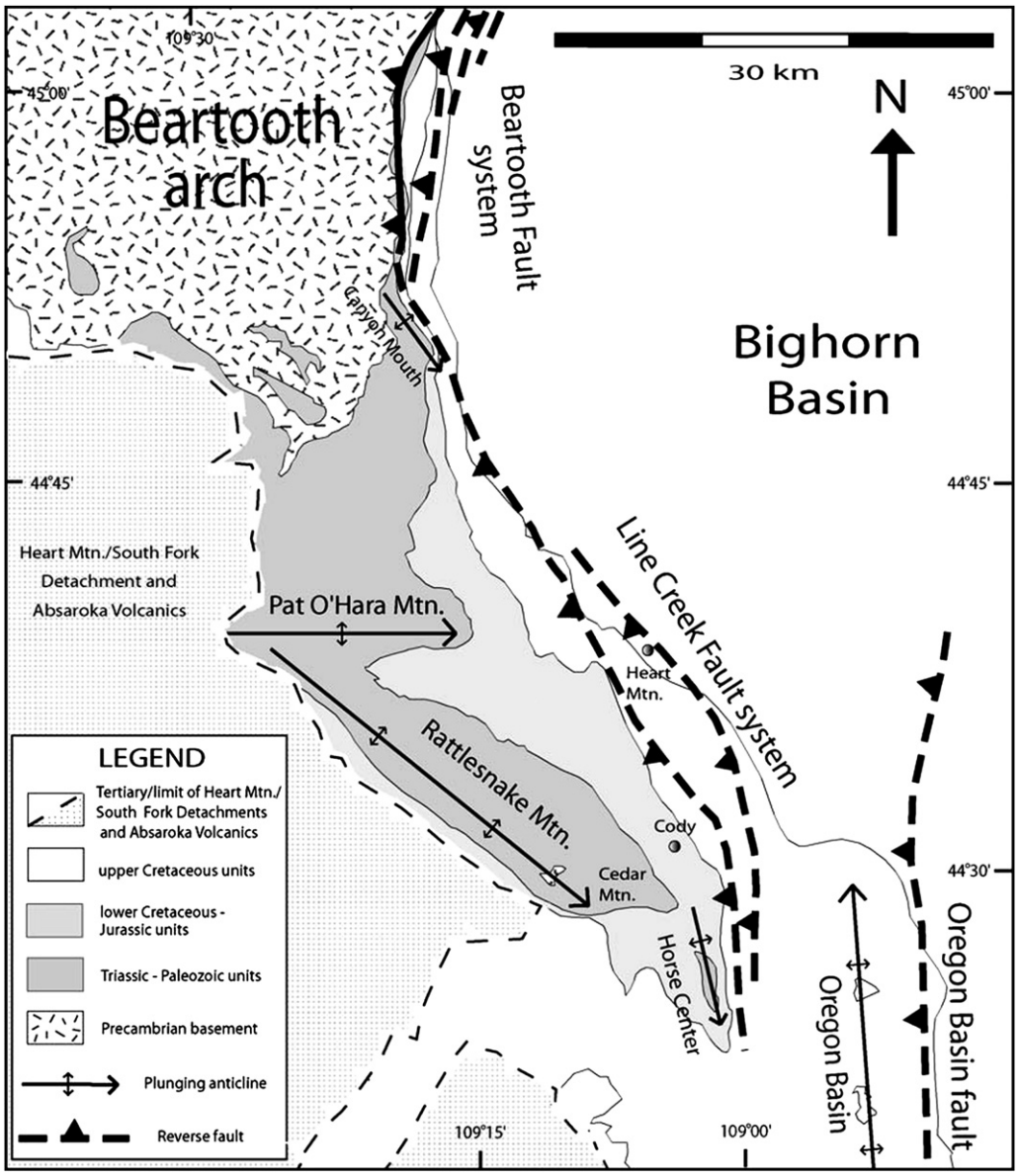

Fig. 2. Simplified geologic map of the NW Bighorn Basin including primary fault systems, primary and secondary folds, and exposures of Precambrian basement rocks (after Love and Christiansen, 1985).

fault systems) to secondary anticlines with N-, NW- and E-trends. This arch transition has been used as a type location for vertical tectonic models of block faulting (Stearns, 1971), fold-thrust deformation during horizontal shortening (Blackstone, 1986), and rotational fault-bend folding of basement blocks during horizontal shortening (Erslev, 1993).

This study documents the 3D geometry and kinematic development of this basement-involved foreland arch transition and uses these geometric and kinematic insights to test hypotheses concerning the roles of local versus regional processes at arch transitions. Specifically, are along-strike changes in arch geometry controlled by reactivation of pre-existing basement structures, changes in the orientation of arch vergence or shortening amount, or by the linking of two or more arches? This study documents the kinematics of the southern Beartooth arch transition (Fig. 2) by (1) collecting minor fault data to document slip and paleostress directions, (2) defining the transition's 3D structural geometry using extensive surface and subsurface data, and (3) testing and refining this geometry by balancing 2D cross-sections and derivative 3D surfaces. Thin-skinned gravity sliding features due to the Heart Mountain (Hauge, 1993) and South Fork (Clarey, 1990) detachments have not been included in the cross-sections and 3D models as the intent of this study is to examine the basement-involved Laramide structures. The results show a complex yet understandable interplay of multiple fold mechanisms controlled by both regional shortening direction and local pre-existing weaknesses.

2. Regional setting

Within the region surrounding the southern Beartooth arch and northwestern Bighorn Basin, approximately 7 km of Cambrian to Tertiary sedimentary rock units nonconformably overlie Precambrian crystalline basement (Johnson, 1934; Pierce, 1966; Pierce and Nelson, 1968; Fig. 3). The Phanerozoic sedimentary section is characterized by strong Paleozoic limestones and weak Cretaceous

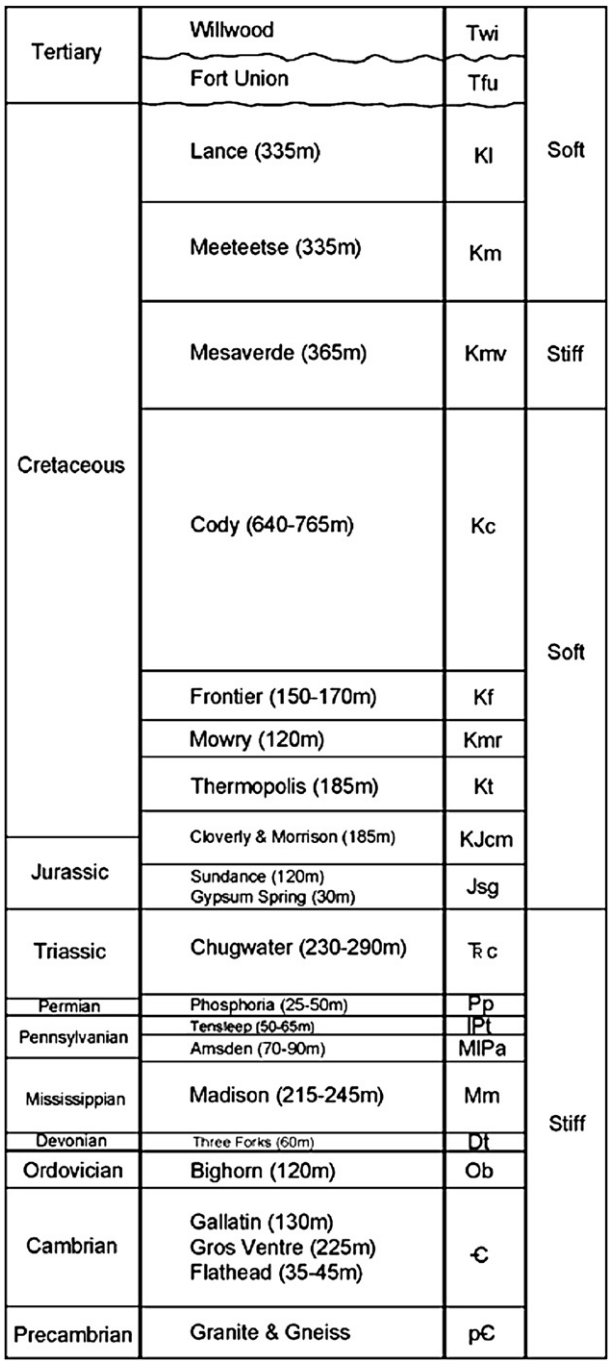

Fig. 3. Generalized stratigraphic column of Precambrian through early Tertiary rocks of the Bighorn Basin (from Durdella, 2001). Note: combined thickness of Tertiary units varies from several hundreds to several thousands of meters throughout the Bighorn Basin.

shales overlain by synorogenic terrestrial clastic units of Paleogene age (Pierce, 1966; Pierce and Nelson, 1968; DeCelles et al., 1991).

The northwest margin of the Bighorn Basin juxtaposes structurally high Precambrian crystalline rocks and Paleozoic sedimentary rocks against the Mesozoic and Tertiary sedimentary strata exposed in the basin. Seismic data across this structural margin ubiquitously show west-dipping no-record zones offsetting the lower Paleozoic strata (Stone, 1985), which we interpret as fault zones. These basin-boundary faults include the partially exposed splays of the Beartooth Fault on the east flank of the Beartooth arch and the blind Line Creek and Oregon Basin faults (e.g., Blackstone, 1986). The blind thrusts are revealed at the surface by abrupt steepening of Cretaceous units to dips of 40°–60° and on-lapping, synorogenic Paleogene basin fill.

The Amoco #1 well, located on the NE corner of the Beartooth arch, drilled through 2.5 km of Precambrian basement before passing through the Beartooth thrust into Cretaceous strata, demonstrating lower angle (10–15°) thrust faulting in this area (Wise, 2000). West of this basin-bounding thrust system, three significant folds are developed along the southeast margin of the Beartooth arch (Fig. 2). Roughly 20 km to the south, the hanging wall of the Beartooth Arch is folded into an anomalously E–W oriented, east-plunging, south-facing structure known as Pat O'Hara Mountain anticline (Fig. 2). The western termination of this anticline exposes the Mississippian Madison Limestone, which is gently folded and smoothly transitions into the crest of the NW-trending Rattlesnake Mountain anticline (Fig. 2).

The NW-trending, 27-km-long Rattlesnake Mountain anticline is the largest, best exposed, and most well-known anticline in the area, and perhaps in the entire Laramide Province. This structure is asymmetric, with a steep, SW-facing forelimb and a nearly planar, 12°–15° NE dipping backlimb. The uniformity of backlimb dips and the associated scarcity of minor faults and folds within outcrops of Precambrian basement indicate that little, if any, penetrative folding of the basement rocks occurred at Rattlesnake Mountain anticline during the Laramide (Erslev, 1990). Stearns (1971) and Erslev (1990, 1993) showed that surface exposures along the Rattlesnake Mountain structure could be largely explained by translations and rotations of rigid basement blocks along curved faults. At Shoshone Canyon west of Cody, Wyoming, basement rocks are faulted against tilted Cambrian and Ordovician rocks of the anticlinal forelimb on a steeply-dipping (86° SW) basement fault. Although early workers cited this exposure as clear evidence that many Laramide uplifts were formed by large amounts of dip-slip motion along near-vertical faults (Stearns, 1971, 1975, 1978), subsequent studies used balancing constraints to demonstrate that the exposed, steeply-dipping fault is better interpreted as a relatively minor splay off a reverse fault (Brown, 1984; Stone, 1984; Erslev, 1986) that merges with the east-verging Line Creek Fault system at depth (Fig. 2) (Erslev, 1990).

Rattlesnake Mountain anticline terminates to the SE at Cedar Mountain in an abruptly-plunging anticlinal nose, which curves east into the smaller, tighter Horse Center anticline (Fig. 2). The structural culmination at the 10-km-long Horse Center anticline is 1–1.5 km lower than at Rattlesnake Mountain, with the lowest exposed stratigraphic level in the Triassic Chugwater Formation. The geometry of Horse Center anticline is well constrained by abundant drill hole and seismic data (e.g., Durdella, 2001). These data show that the Horse Center anticline is cored by a west-dipping basement fault, with several shallow, east-dipping back-thrusts controlling much of the fold geometry in the cover rocks exposed at the surface.

East and south of Horse Center anticline, the western margin of the Bighorn Basin is marked by the Oregon Basin anticline. Seismic data through this structure indicate that the Oregon Basin anticline developed above a west-dipping thrust fault that offsets the basement nonconformity with approximately 6 km of throw (Stone, 1984). This structural geometry is similar to exposures of the Beartooth margin to the north.

3. Minor fault kinematics

Minor faults provide an important tool to determine regional shortening and paleostress. They can be used to identify multiple directions of regional shortening and can indicate the relative

timing and importance of sequential stages or discrete periods of deformation. Moreover, minor faults can be used to indicate the optimal orientation(s) for constructing and restoring cross-sections as well as the possibility of localized vertical axis rotations, which can be indicated by local deviations in regional shortening directions (Erslev and Larson, 2006).

Slickensided minor faults are common in tilted sandstone units throughout the northwestern margin of the Bighorn Basin, particularly in the Pennsylvanian Tensleep Sandstone within steeply-dipping anticlinal limbs. Minor faults typically occur as 1–10 mm thick zones of highly-striated, quartz-rich cataclasite that lack clay gouge and crop out either as erosionally-resistant shear bands or as discrete outcrop surfaces. They can occur in sets of cross-cutting thrust or strike-slip conjugate pairs, spaced from several meters to several millimeters apart. Where thrust and strike-slip faults occur together, they share a common acute bisector, suggesting one direction of maximum shortening and compression.

Slip and orientation data from 1581 minor faults were collected from 24 data stations both within and away from anticlinal hinges and forelimbs (Figs. 4 and 5). Slip sense was determined in the field using the criteria of Petit (1987). Ideal Compton (1966) σ_1 orientations were calculated for each fault using an α angle (half the acute bisector of conjugate faults) value of 20°, which most closely fits the conjugate faulting patterns of rock units within the study area (Neely, 2006) and elsewhere in the Rockies (e.g., Erslev, 2001; Erslev and Larson, 2006). Average fault plane, slickenline, and ideal σ_1 orientations for each data set were calculated using eigenvector analyses, with eigenvalues used to quantify data scattering (Table 1). Rose diagrams of ideal σ_1 trends were smoothed with a 10° window such that values for each degree represent all data within 5° of the target value (Fig. 5). More details about these analyses are contained in Neely (2006).

Minor fault patterns were analyzed in their current orientations as well as in their orientations with bedding restored to horizontal. Whereas minor faults are commonly oblique to bedding, ideal σ_1 orientations show a strong correlation with bedding attitude, with the average σ_1 orientation for most stations lying approximately on that station's bedding plane. Thus, when fault and σ_1 data are rotated about the bedding strike to horizontal, most stations show subhorizontal ideal σ_1 orientations. This suggests that minor faulting occurred when bedding was subhorizontal or that compression during deformation was aligned approximately parallel to bedding.

Inferred ideal σ_1 orientations are most strongly clustered at the four stations situated away from anticlinal limbs and the four northernmost locations on the east flank of the Beartooth arch, with the first eigenvalue (E_1) ranging from 0.9785 to 0.8191 (Fig. 4b; black rose plots with solid lines to stereonets in Fig. 5). These sites are the most internally consistent group of stations, with average ideal σ_1 orientations agreeing within 7° and giving an overall average orientation of 065°. This orientation is consistent with other estimates of regional Laramide shortening and compression directions (Bolay-Koenig and Erslev, 2003), and is therefore interpreted as the regional shortening and compression direction for the area.

The three sites located within the steeply south-dipping forelimb of Pat O'Hara Mountain anticline show ideal σ_1 trends of 020–025°. This direction is oblique to both the axis of Pat O'Hara Mountain and the regional shortening direction of 065°. Although fault data from these three locations show a great diversity of fault plane and slickenside lineation orientations, their ideal σ_1 orientations are well clustered, with intermediate eigenvalues (E_1: 0.7187, 0.6617, and 0.6049).

Two sites (EF1 and EF3) located on the N–S-trending segment of the southern Beartooth arch also exhibit ideal σ_1 orientations oblique to local fault strike. The acute bisectors of strike-slip and thrust fault conjugate pairs at EF3 are oblique to bedding dip, resulting in an inferred slip direction similar to the 065° signature observed at off-axis locations.

Rattlesnake Mountain anticline shows overall ideal σ_1 orientations approximately perpendicular to fold trend (219°), which is 26° oblique to the regional 065° trend. Many of the stations show bimodal ideal σ_1 orientations suggesting a partitioning of slip on this structure.

3.1. Implications for regional kinematics

Minor fault data can be used to falsify several hypotheses for the kinematics of the region. First, data distant from anticlinal axes indicate single, uniform shortening and compression directions, and are thus incompatible with multi-stage, multi-directional shortening hypotheses. Second, the Pat O'Hara Mountain data show that early shortening was not perpendicular to all fold trends, and that Pat O'Hara Mountain anticline did not form perpendicular to our interpreted regional stress directions. Instead, the data suggest that oblique-slip occurred on faults underlying this, and possibly other structures, like the NW-trending Rattlesnake Mountain anticline.

Along the east flank of the Beartooth arch, fault data proximal to the primary fault system at stations EF1 and EF3 show shortening and compression parallel to the regional shortening direction. These data suggest that the N–S trending east flank of the southern Beartooth arch is associated with an oblique-slip fault segment. In contrast, faults from stations EF1 and BH4 on the east flank of the Beartooth arch at Canyon Mouth anticline are tightly-clustered, high-angle strike-slip faults and shear bands that suggest a more N–S shortening directions (011°, 215°). Together, the data from these four stations may represent an oblique-slip system that has been partitioned into N–S-oriented strike-slip (stations BH1 and EF4) and E–W oriented (stations BH1 and EF4) shortening components. Similar partitioning has been documented at oblique convergent margins (Yu, 1993) and was suggested by Varga (1993) as an explanation for divergent shortening directions in other Laramide structures.

The shortening directions documented at Rattlesnake Mountain, Pat O'Hara Mountain, and Canyon Mouth anticlines, which are oblique to both local fold axes and the 065° regional shortening direction, may be explained by 1) local, folding-related stress refraction and/or 2) local rigid body rotations about a vertical axis. At Pat O'Hara Mountain, the widely-scattered (000°–070°) but dominant 023° shortening signature can be interpreted as the result of fold-related stress refraction or local material rotation within a zone of left-lateral oblique-slip. The latter hypothesis predicts that the faults related to early shortening and compression about a 065° orientation were progressively rotated counterclockwise about a vertical axis. At Rattlesnake Mountain and Canyon Mouth anticlines, however, shortening directions are approximately perpendicular to the fold trend, suggesting that folding-related stress partitioning was responsible for their deviations from regional shortening and compression directions.

In summary, minor faults measured at stations distant from secondary anticlinal structures indicate a single, regional 065° shortening and compression direction. Because all three of the secondary structures in the area (Canyon Mouth, Pat O'Hara, and Rattlesnake Mountain anticlines) show shortening directions oblique to the interpreted regional shortening direction, data away from secondary structures may provide the best opportunities to identify regional shortening and compression directions. These stress and strain fields appear to have been partially deflected by strain partitioning, vertical axis rotations and/or stress refraction in

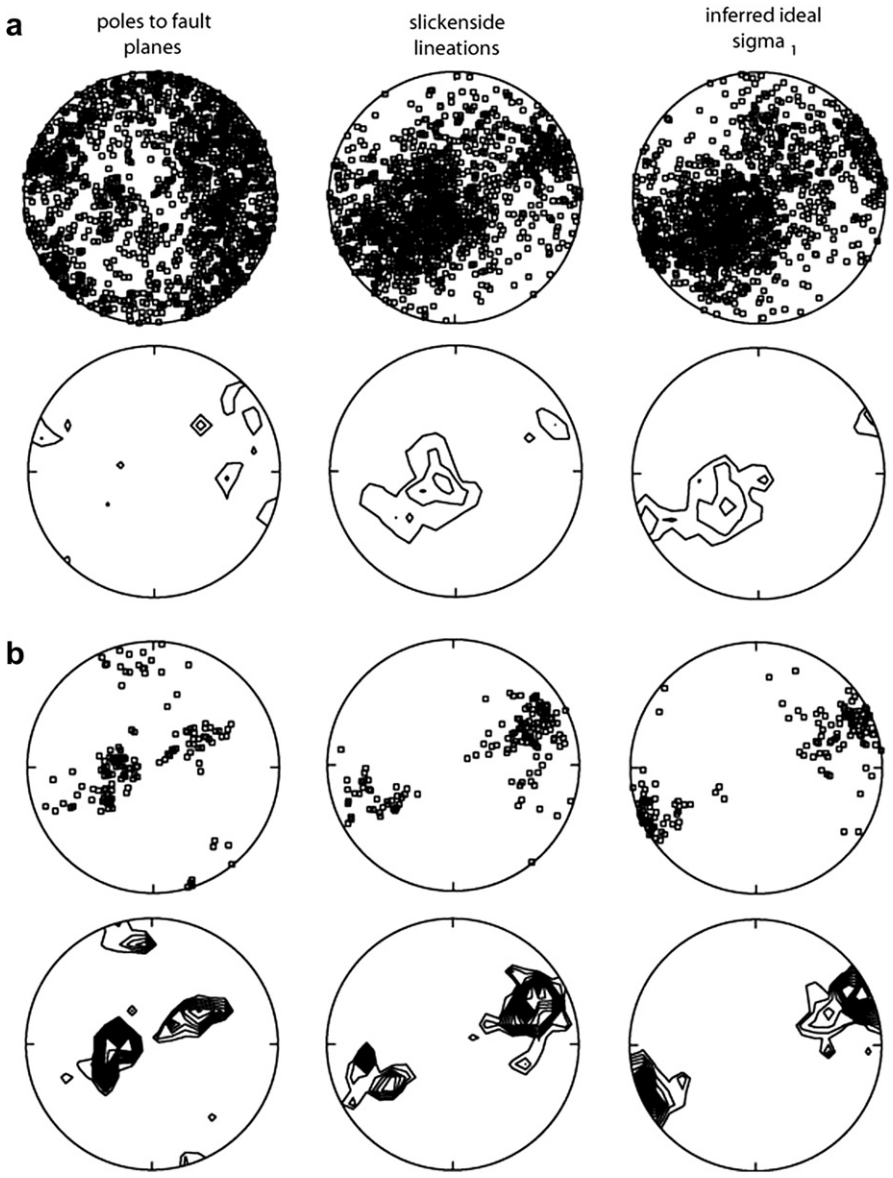

Fig. 4. Stereonet plots showing poles to minor fault planes, slickenside lineations, inferred ideal σ_1 orientations, and their respective contour plots for (a) all minor faults, and for (b) minor faults from the four stations located away from steeply-dipping fold limbs (see text for details). Contour plots are at 4% contour interval (a) and 0.8% contour interval (b).

the oblique-slip Canyon Mouth, Pat O'Hara and Rattlesnake Mountain anticlines. These deflections are consistent with pre-existing basement weaknesses controlling the location of these anticlines.

4. 2D structural geometries and kinematics

In order to further constrain the kinematics of this complex margin, we used 2DMove™ to construct 16 serial cross-sections paralleling the inferred 065° regional shortening and compression direction (Figs. 6 and 7). The cross-sections are constrained by new 1:12,000 field mapping within the hinges and forelimbs of the Rattlesnake Mountain and Pat O'Hara Mountain anticlines (Neely, 2006), previous 1:62,500 geologic mapping (Pierce, 1965a,b, 1966, 1970; Pierce and Nelson, 1968, 1969), publicly available industry well data from 173 wells, and over 1000 km of proprietary industry 2D seismic data (Fig. 6). Structural geometries of the post-Laramide Heart Mountain and South Fork detachment systems are not included in the sections. Geometries in these areas are reconstructed from the orientations of stratigraphy beneath the detachments.

The sections were further constructed and restored in 2DMove using a combination of line-length unfolding, fault-parallel flow combined with inclined shear and trishear fault-propagation folding restoration algorithms, with line length and area balance maintained where appropriate. Although thickness changes are observed in outcrop within the shale-rich Cambrian units adjacent to the Rattlesnake Mountain basement fault in Shoshone Canyon, no obvious indications of significant thickness changes are present in the overlying strata, suggesting that line-length balancing is an appropriate assumption in the sedimentary strata. Area balancing of the Precambrian basement was accomplished by a combination of fault-parallel flow and inclined shear, with a backwards shear applied to simulate rotational motions of larger basement blocks and a forward shear to match the nonconformity dips seen in smaller basement wedges. Trishear folding at the tip of domains of

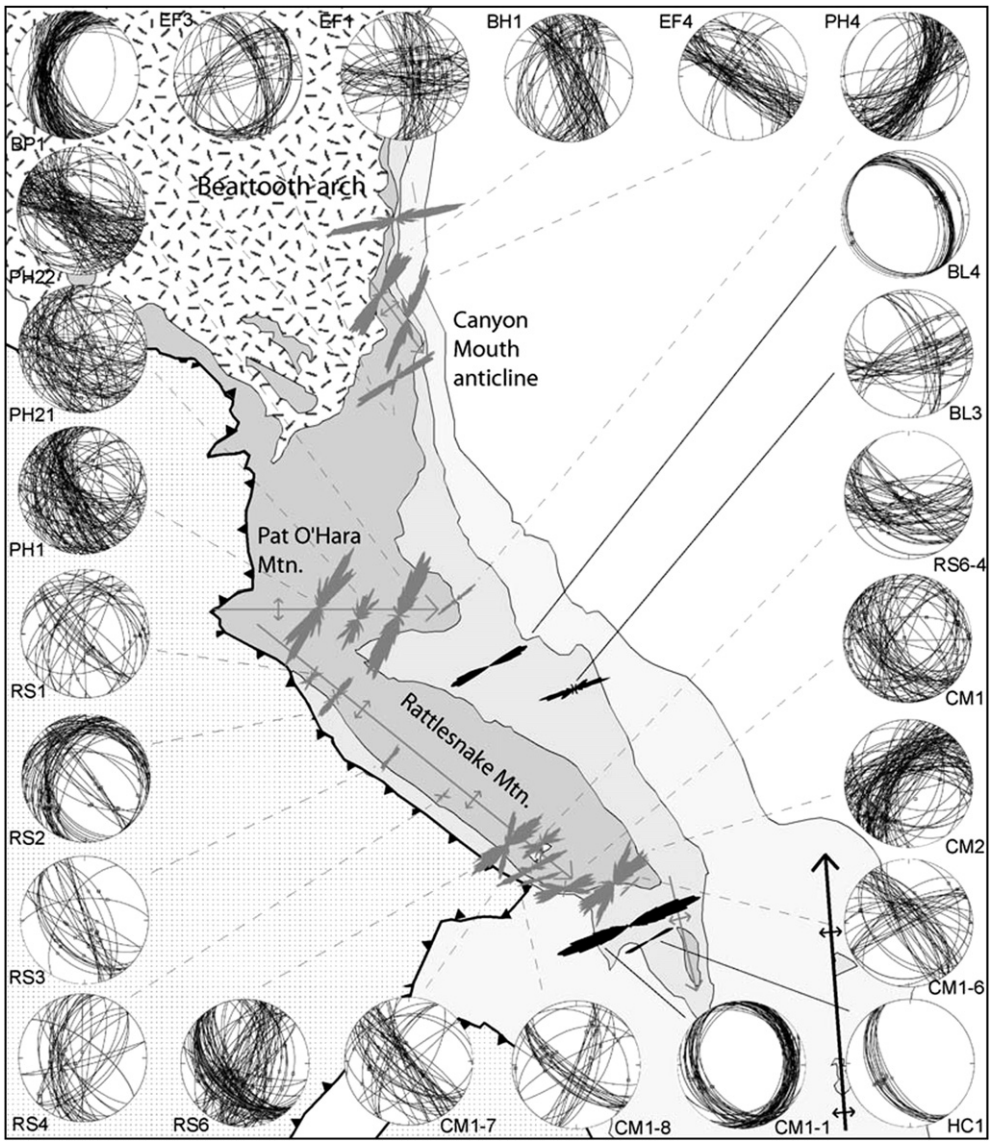

Fig. 5. Map showing fault plane orientations, slickenside lineations (stereonets), and average ideal σ_1 orientations (rose plots) of the 24 minor fault stations. Black rose diagrams represent stations located away from steeply-dipping fold limbs and grey rose diagrams represent stations located within steeply-dipping fold limbs. Geologic map units and scale are the same as in Fig. 3.

fault-parallel flow allowed the modeling of basement folding in front of propagating basement faults.

4.1. Beartooth/Line Creek/Oregon Basin fault systems

4.1.1. Along-strike changes in structural geometry

Seismic and well data document dramatic along-strike changes in the geometry of the eastern margin of the Beartooth arch. Although seismic and balancing data indicate that the dip of the major arch-bounding faults is typically between 40 and 50°, these faults differ in number, slip distribution and the degree to which they fold the basement nonconformity. In the north, the Beartooth fault system comprises four faults (Fig. 7, cross-sections A–A′ and B–B′). These include three blind, gently east-dipping fault blocks basin-ward of the range-bounding fault that is exposed at the surface. Immediately south, slip on these four splays of the Beartooth fault system was transferred to a single fault dipping ~50° SW (sections D–D′ to F–F′, Fig. 7). In the central area (sections G–G′ to O–O′, Fig. 7), slip on the Line Creek fault system was distributed between two faults, as indicated by the presence of an intermediate basement fault block, with overlying beds dipping ~25° to 30° NE. In the south, two sub-parallel thrust faults bound the east side of the Horse Center and Oregon Basin (Stone, 1984) anticlines and display moderate SW dips similar to those of the Line Creek and Beartooth fault systems. West-directed faults on the west side of these two structures appear to be backthrusts, which locally pick up chips of basement. South of Oregon Basin anticline, basement deformation within the hanging wall of the western margin of the Bighorn Basin is distributed among numerous, widely-spaced basement backthrusts, forming a gently folded, NE-dipping hanging-wall surface (Hennings and Hager, 1996).

4.1.2. Basement folding

Folding of the basement surface proximal to the Line Creek fault system is present in two areas. In section E–E′ (Fig. 7), where the Line Creek fault system occurs as a single fault splay, a sharp increase in the eastward dip of surface bedding and well dips documents a gently folded basement surface above the Line Creek

Table 1
Station names, UTM coordinates (UTM zone 12 north, North American Datum 1927), average ideal σ_1 orientations (current orientations and rotated orientations with bedding horizontal), and eigenvalues for average ideal σ_1 orientations for each minor fault collection location. Asterisk (*) indicates overturned bedding.

Station	UTM (*X*)	UTM (*Y*)	Number (#)	Bedding	Average σ_1	Eigenvalue	Rotated σ_1
BH1	634209	4968767	70	345/70	010/44	0.8463	215/03
BP1	634801	4962668	2	015/39	177/07	0.961	356/06
CM1	645733	4927221	67	113/57	267/24	0.7069	079/06
CM2	647556	4927345	102	078/28	228/20	0.7359	223/05
CM1-6	649383	4927454	28	068/15	341/69	0.6467	350/84
PH1	630827	4945152	106	095/77	232/57	0.7187	103/41
PH2-1	632719	4945119	81	098/71	216/49	0.6049	027/17
PH2-2	632374	4945181	111	096/83	234/63	0.6617	026/11
PH4	637797	4946276	20	330/21	053/06	0.8581	233/15
CM1-7	645054	4927622	46	130/70	294/62	0.7544	247/11
CM1-8	644632	4927902	31	131/59	262/34	0.5606	075/15
RS1	627918	4942126	34	134/76	229/60	0.5704	047/16
RS2	630003	4942126	60	132/79	238/34	0.6512	060/43
RS3	634116	4935791	24	137/49	207/68	0.7403	219/20
RS6	642899	4929217	101	136/48	214/56	0.6711	219/08
RS4	638808	4932297	33	307/69*	232/49	0.6419	056/60
BL3	649602	4938589	38	341/55	067/40	0.8107	248/15
BL4	640358	4941968	29	308/17	064/16	0.9785	063/01
CM1-1	649818	4925013	62	110/16	248/03	0.9481	068/08
HC1	651767	4925934	12	146/40	241/36	0.9277	060/04
RS6-4	644068	4929296	49	151/17	228/70	0.8634	234/53
EF1	633674	4972731	65	004/62	064/57	0.8448	258/01
EF3	635167	4965069	50	016/30	036/28	0.8402	047/14
EF4	635541	4966247	61	303/70	339/63	0.8765	011/03

hanging wall. In sections J–J′ and K–K′ (Fig. 7), surface dip and well top (well 2921417) data indicate that the subhorizontal basement surface west of the Line Creek fault system is abruptly folded as it approaches the western of the two Line Creek faults.

4.1.3. Detachment folding and triangle zones

Within the hanging wall of the Line Creek fault system, several west-facing anticlines (Fig. 7: Heart Mountain anticline in sections H–H′ and I–I′, Fish Hatchery anticline in sections J–J′ and K–K′, Cottonwood and Shoshone anticlines in L–L′, M–M′ and N–N′) display geometries that indicate detachment faulting within Mesozoic strata above the emergent Line Creek fault system. These faults are interpreted as thin-skinned backthrusts and define a triangle zone above the Line Creek faults.

4.2. 2D connections between basin-bounding fault systems and hanging-wall anticlines

Two principal lines of evidence suggest that the fault underlying Rattlesnake Mountain is kinematically linked to the Line Creek Fault system. First, the basement surface of the Line Creek hanging wall is at a lower elevation near the fault cutoff than the basement surface of the Rattlesnake Mountain footwall block (particularly in cross-sections G–G′, H–H′ of Fig. 7). Such geometry requires either fault inversion (i.e. normal faulting, for which there is no evidence) or down-to-the-NE rotation of the Line Creek hanging wall. In an area balanced model of this geometry, this down-to-the-NE rotation would require a complementary up-to-the-SW rotational component, and the most likely candidate for this complement would be the Rattlesnake Mountain structure. Second, much of the Rattlesnake Mountain backlimb is uniformly tilted from anticlinal crest to its cutoff by the Line Creek fault system. This suggests that rotational block movement of the Rattlesnake Mountain hanging wall occurred on a curved, concave-up fault.

A balanced rotational fault block model in which the Rattlesnake Mountain fault curves concave-upward into the eastern of the two Line Creek faults restores the basement surface reasonably well to its hypothesized pre-faulting geometry (Fig. 8). 2D rotational modeling suggests that the eastern Line Creek fault is well-positioned to be related to early rotation of the Rattlesnake Mountain block, whereas the western Line Creek fault could not be modeled using rotational basement blocks and reasonable fault dips. This suggests that the western Line Creek fault post-dated backthrusting on the Rattlesnake Mountain fault. The differentiation of these two faults could be the result of block rotation moving the eastern splay of the Line Creek fault system out-of-plane with the underlying Line Creek master fault, which then finally broke through to the west on the western fault splay. Alternatively, the apparent two-stage development of the Line Creek fault system could reflect 3D strain accommodation within the southern Beartooth arch transition, possibly expressed as a relay ramp or step-over structures (see 3D discussion below).

These models and restorations, combined with the observation of basement folding near the Line Creek Fault zone, suggest the following kinematic sequence of faulting (Fig. 8) within the Line Creek and Rattlesnake Mountain fault systems: 1) basement arching to the west (Fig. 8a and b) associated with deep-seated slip on the Line Creek fault, whose tip propagated toward the basement-cover nonconformity; 2) Rattlesnake Mountain backthrusting in response to the slowing or arresting of Line Creek Fault-propagation (Fig. 8b and c), causing (a) synchronous up-to-the-SW rotation of the Rattlesnake Mountain hanging wall and down-to-the-NE rotation of the Line Creek hanging wall and (b) basement folding forming a hinge line where the eastern-most splay of the Line Creek Fault would eventually cut the basement nonconformity; and 3) propagation of the western splay of the Line Creek fault system into the Paleozoic strata and the ceasing of slip on the Rattlesnake Mountain thrust (Fig. 8d).

5. 3D geometries and kinematics

The areas linking the southern Beartooth arch, Rattlesnake Mountain anticline and Oregon Basin fault provide insights into the controls and mechanisms of slip transfer from one basement-involved structure to another. To better understand these processes and geometries, we used 3DMove to create 3D models of six

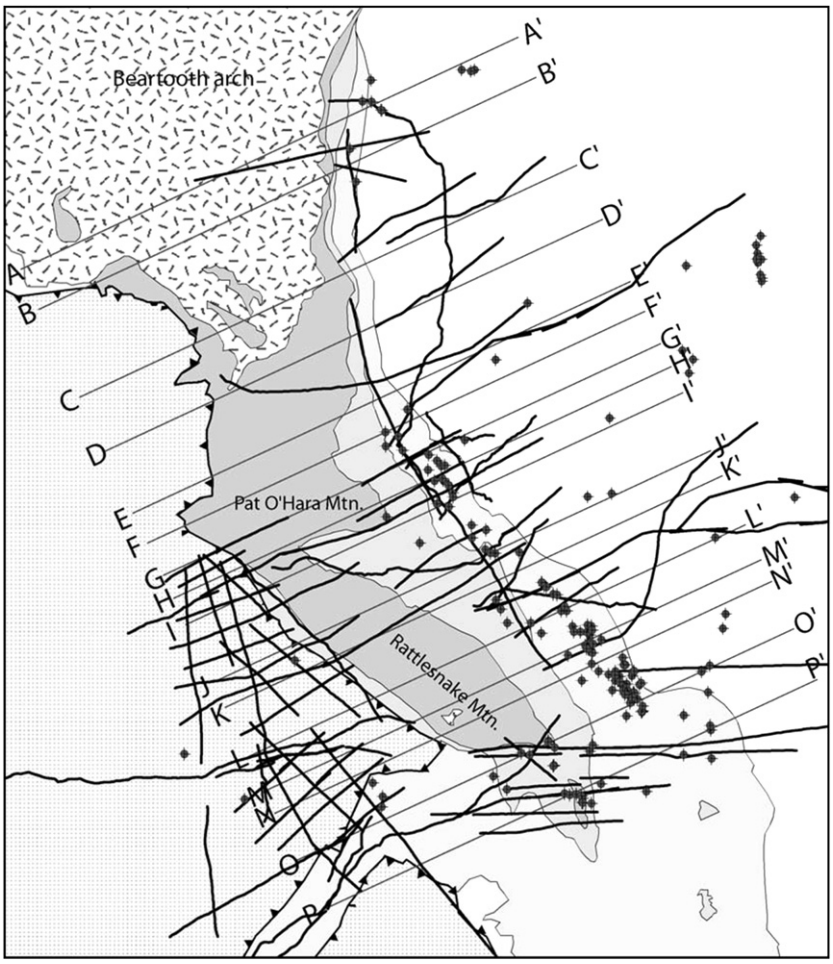

Fig. 6. Map showing locations of the 16 cross-sections constructed in this study, proprietary industry seismic data (bold lines), and well data used in this study. Geologic map units and scale are the same as used in Fig. 3.

stratigraphic horizons throughout the region. The Precambrian basement surface was then restored and used to interpret the 4D kinematic and geometric development of this arch transition zone. For each stratigraphic surface, a 3D model was created that honors the 2D cross-section data, surface exposures of folds, fault offsets, and individual and branching fault blocks (see Fig. 9 for the basement and partially extrapolated Frontier surfaces; see Neely (2006) for the 4 intervening surfaces). The basement surface was restored parallel to the regional shortening direction (065°) using 3DMove's flexural slip flattening algorithm, with pin walls aligned approximately perpendicular to structural trends in areas of minimal distortion. The resulting flattened surface (Fig. 10) was reconstructed using a jigsaw restoration approach which tried to minimize overlaps and gaps within the restored surface. These were used to evaluate the geometric validity of the interpreted surface and its consistency with hypotheses concerning the general kinematic framework.

5.1. Transitions between the Beartooth, Line Creek and Oregon Basin fault systems

The southern plunge of the Beartooth arch along the NW margin of the Bighorn Basin is expressed at the surface as a decrease in the elevation of the hanging-wall basement nonconformity. This change in maximum structural elevation is paralleled by a nearly equivalent southward decrease in the elevation of the footwall basement nonconformity in the Bighorn Basin directly to the east. The overall throw at the Bighorn Basin margin, as measured from west of hanging-wall backthrusts to the floor of the basin, decreases southward from the Beartooth fault system to the Line Creek fault system. A more pronounced change is observed in the overall throw on the west-dipping faults cutting the basement nonconformity in this vicinity, with throw decreasing from 6 km in the northernmost section (A–A′, Fig. 7) to as little as 2 km in section M–M′.

The 3D geometry of fault splay interactions along the Beartooth, Line Creek, and Oregon Basin fault systems was not clearly resolvable in seismic data, and was constrained principally by interpolating between 2D cross-sections. One N–S-oriented seismic line from the east flank of the Beartooth arch, however, shows that slip transfer on the Beartooth Fault splays can occur via gently south-dipping monoclinal folds of the basement surface.

The Line Creek and Beartooth fault systems display along-strike transitions in both width and number of fault splays. At the northwest boundary of the study area, seismic and well data clearly document at least four fault splays defining a wide, distributed fault zone. Southward, near cross-sections D–D′ and E–E′, seismic data indicate that slip on these four fault splays coalesced into a single fault in a zone interpreted by Blackstone (1986) to be the transition between the southward termination of the Beartooth Fault system and the northwestward termination of the Line Creek fault system. The interpretation that these two

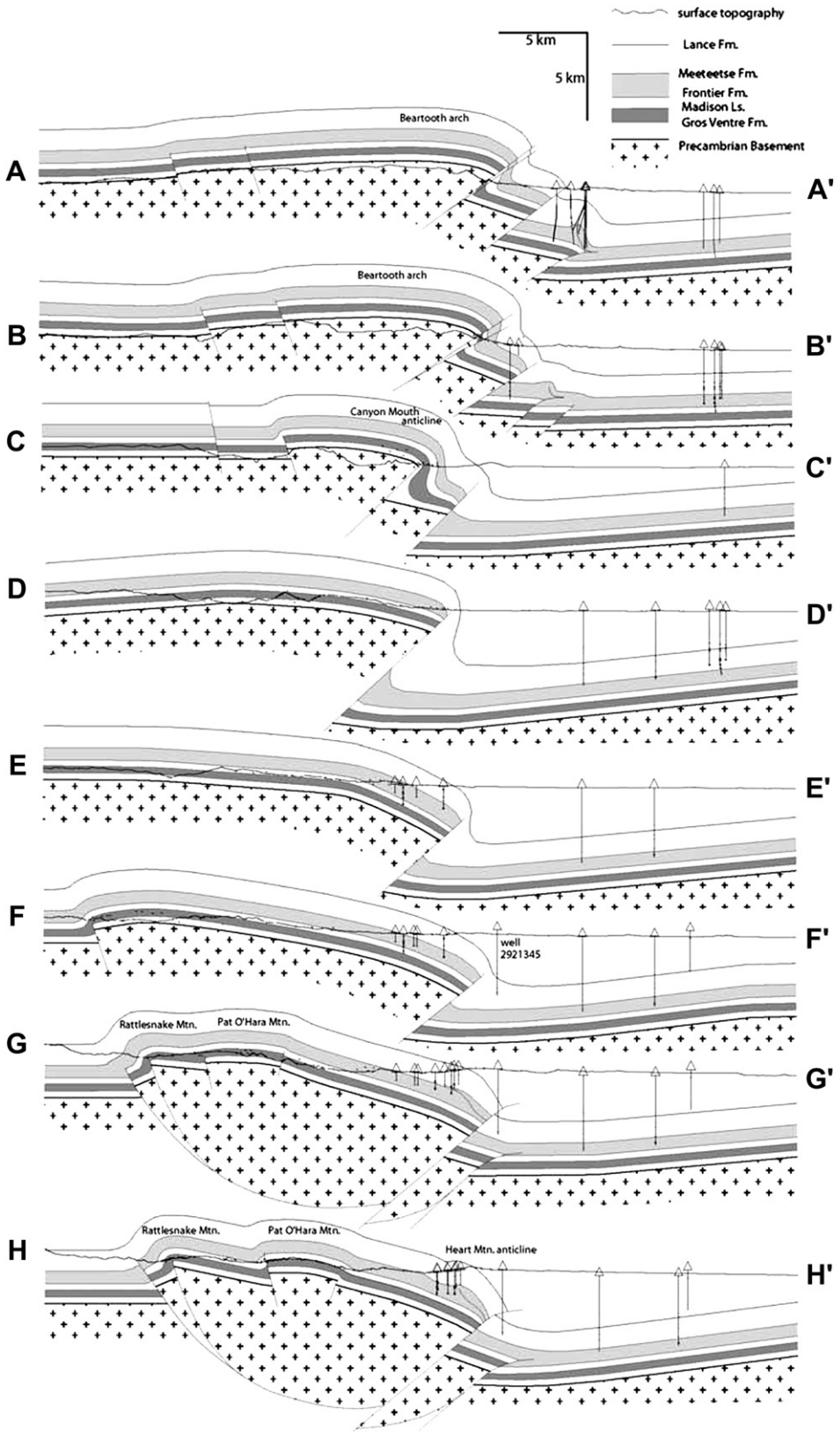

Fig. 7. Cross-sections A–A′ through P–P′ showing interpreted 2D geometries based on surface and subsurface data and restoration constraints. Cross-section, well and seismic data locations are shown in Fig. 6.

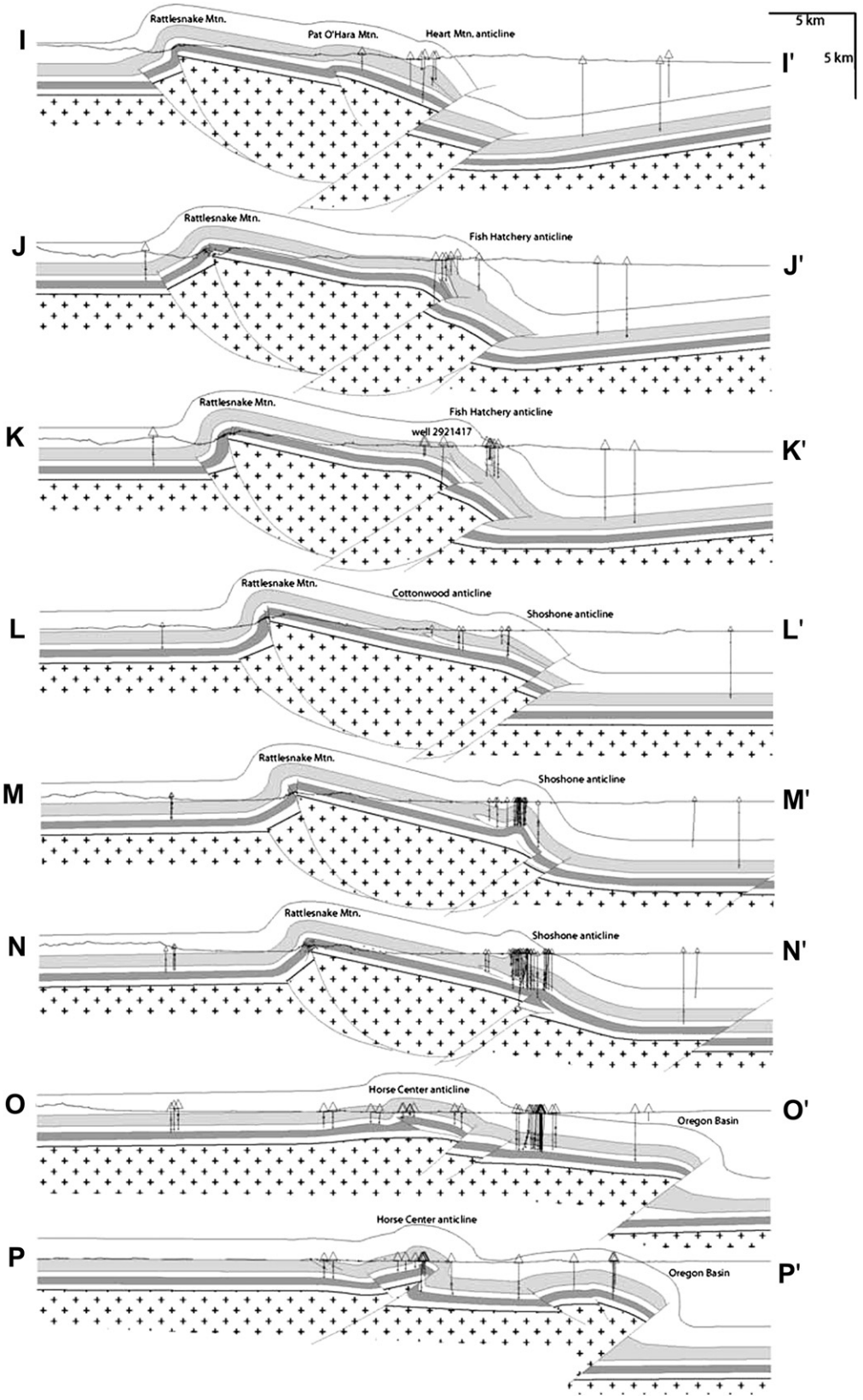

Fig. 7. (*continued*).

faults systems are part of a single system is based on the following observations: 1) the northwest projection of the western Line Creek fault from sections D–D′/E–E′ into the Beartooth fault system in section C–C′ is well defined by seismic data and projects directly into the Canyon Mouth anticline, which is interpreted here as the surface expression of the Line Creek fault, 2) the presence of a continuous, overturned, and unfaulted fold at the level of the Ordovician Bighorn Dolomite above the Line Creek

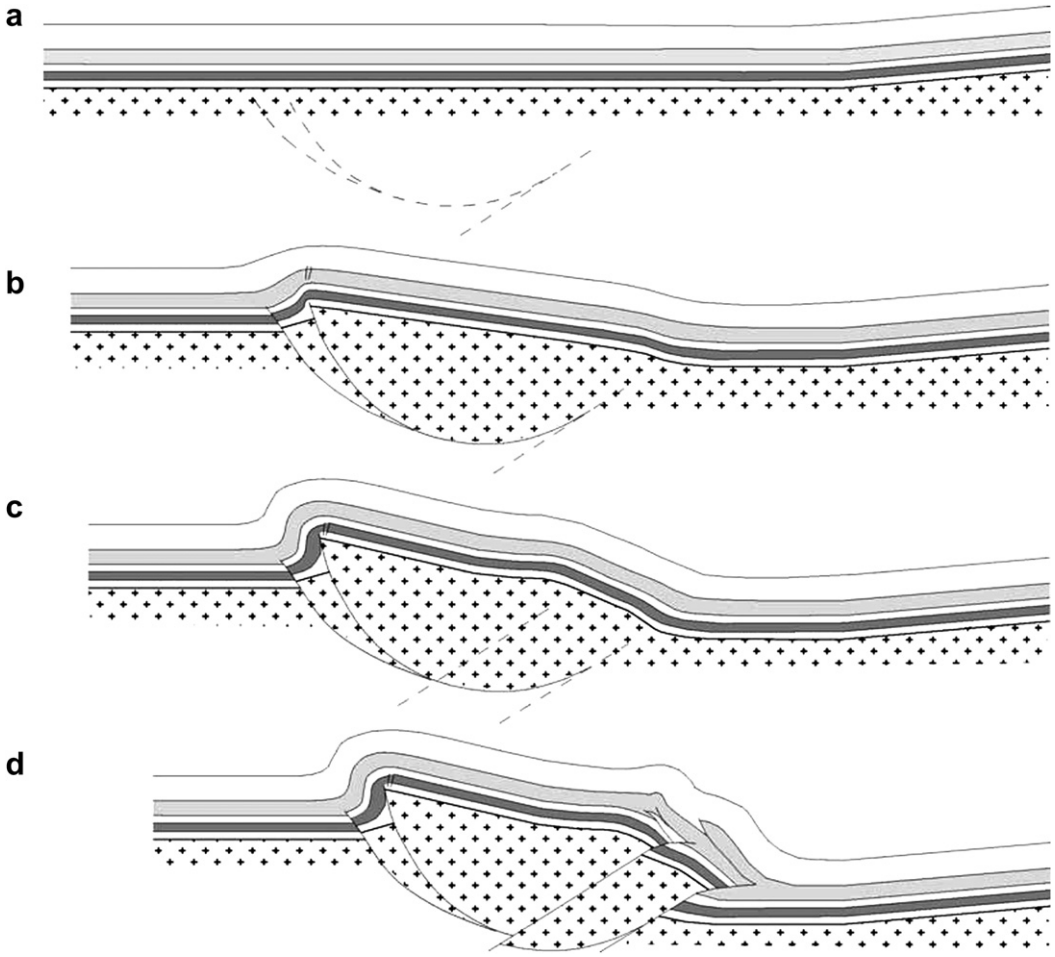

Fig. 8. Balanced rotational basement block model illustrating the proposed development of the Line Creek–Rattlesnake Mountain system.

fault at Canyon Mouth anticline (Fig. 7, section C–C′) suggests that Canyon Mouth anticline distributes slip from one of at least two fault splays in the Beartooth–Line Creek fault system. The easternmost of these two faults is interpreted as the southern extension of the westernmost Beartooth fault splay (Fig. 7; sections A–A′ and B–B′). This fault termination is interpreted as an intermediate level splay of the Beartooth–Line Creek fault near section D–D′.

Southeast of section F–F′, seismic and well (well 2921417) data show the presence of two faults associated with the Line Creek fault system. To the southeast, increased throw on the eastern of these two splays is complemented by a decrease in throw of the western splay (Fig. 9a), suggesting slip transfer to the eastern splay. The geometry of the basement surface in this transfer system resembles a basement-involved compressional relay ramp.

5.2. Pat O'Hara Mountain and northern Rattlesnake Mountain anticlinal intersection

Basement and Cambrian-level exposures between the southernmost Beartooth arch and Pat O'Hara Mountain anticline indicate that the basement nonconformity is subhorizontal until it is folded upward as a part of the north-dipping backlimb of Pat O'Hara Mountain anticline (Pierce and Nelson, 1968). This anticline is much more symmetric than Rattlesnake Mountain anticline, with backlimb dips up to 55° versus maximum backlimb dips of 15° at Rattlesnake Mountain. The backlimb of the fold is cut by a steeply-dipping, 080-striking fault with approximately 100 m of south-side-up throw near the crest of the structure (Pierce and Nelson, 1968). Surface exposures on the east end of Pat O'Hara Mountain define an eastern plunge of 30°–40° into the junction of the Line Creek fault system.

At the western tip of Pat O'Hara Mountain anticline, an abrupt, ~2 km drop in the basement surface elevation occurs at its intersection with the Rattlesnake Mountain anticline, showing a linkage between the two structures. Although much of this intersection is covered by Tertiary volcanic rocks, several limited outcrops near the Rattlesnake Mountain/Pat O'Hara Mountain intersection suggest the apparent westward continuation of Pat O'Hara Mountain anticline (Pierce, 1966; Pierce and Nelson, 1968) and the termination of Rattlesnake Mountain anticline into Pat O'Hara Mountain anticline.

It is tempting to think of the Pat O'Hara Mountain anticline as the result of a transpressive, right-lateral tear fault between the NE-directed Beartooth–Line Creek fault system and the SW-directed Rattlesnake Mountain backthrust. The tighter, more symmetric geometry of the Pat O'Hara Mountain anticline and the high-angle axial fault do resemble a strike-slip flower structure. However, the orientation of the anticline and the apparent counter-clockwise rotations of minor faults in the steeply-dipping forelimb are more consistent with a left-lateral shear sense. Instead, the abrupt termination of the Rattlesnake Mountain and Pat O'Hara Mountain anticlines to the NW (Fig. 10) suggests that the northwest end of these structures may represent a pivot point within the hanging wall. In this case, these folds would represent pleats in the hanging

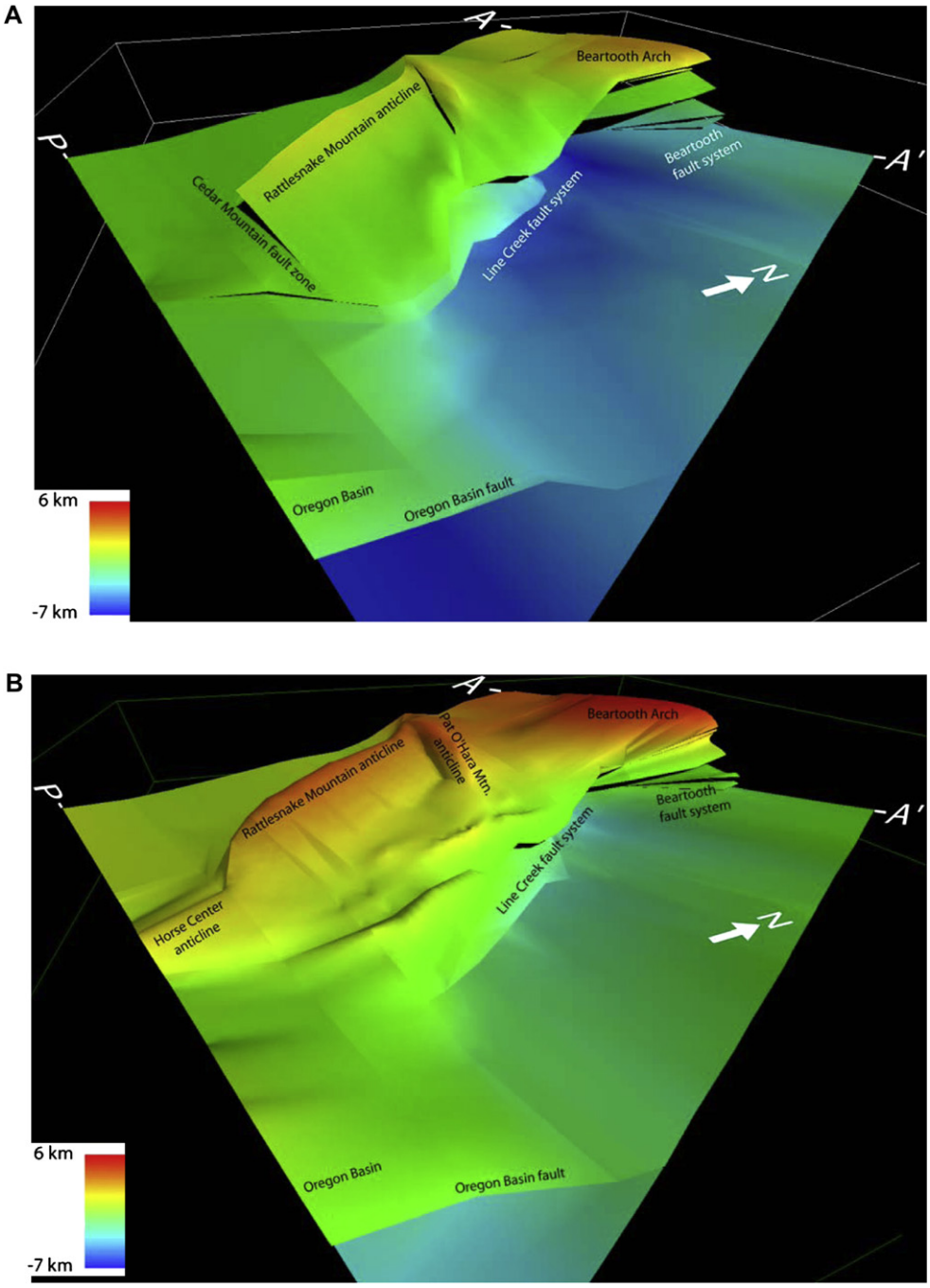

Fig. 9. Three-dimensional views looking NW from the SE corner of the 3DMove model of (A) Precambrian basement nonconformity and (B) top of Frontier Formation surfaces. Surface elevations are indicated by warmer (high) and cooler (blue) colors.

wall that allowed clockwise rotation of the hanging wall to the south of the pivot point during deformation. Coincidentally, the decrease in slip from the Beartooth fault system southward into the Line Creek fault system (Fig. 10) also represents a clockwise rotation of the hanging wall with respect to the Bighorn Basin itself. In this case, however, the rotational pivot point is south of the study area. The fact that the overall horizontal shortening is greater in the Beartooth arch segment of study area than the Line Creek segment suggests that the pivoting within the hanging wall represented by the Pat O'Hara Mountain and Rattlesnake Mountain anticlines is secondary to the larger pivoting on the master Beartooth–Line Creek fault systems.

5.3. Cedar Mountain fault zone

A complicated structural transition occurs along the southern margin of the Beartooth arch, where Rattlesnake Mountain anticline terminates at Cedar Mountain. Here minor fault data (location CM2, Fig. 5) and the steep, southerly plunge of Rattlesnake Mountain anticline suggest left-lateral motion along the south flank of Cedar Mountain. We propose that this left-lateral motion is related to a basement tear fault that we here name the Cedar Mountain fault zone (Fig. 9). Restoration of the basement surface (Fig. 10) supports our tear fault hypothesis because the amount of basement surface shortening in Rattlesnake Mountain anticline

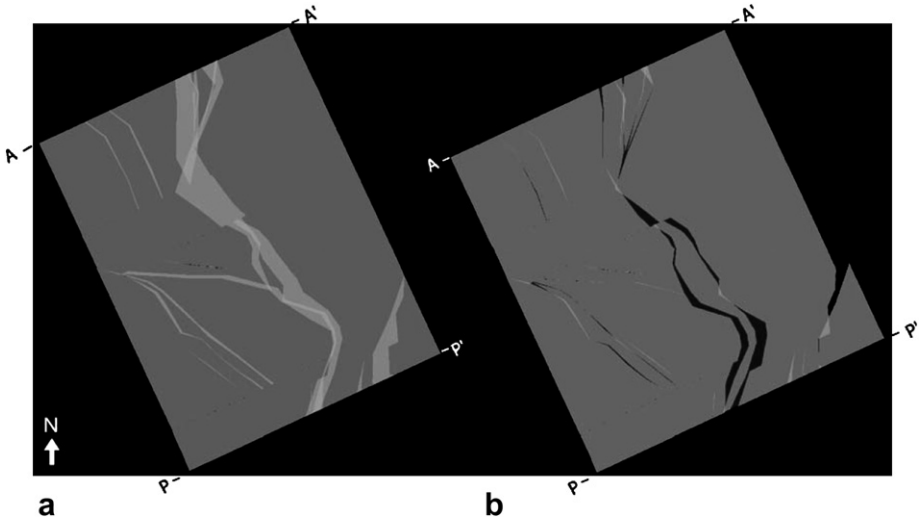

Fig. 10. Flattened basement surfaces with fault heaves unrestored (a) and restored (b). Lighter areas indicate surface overlaps and black areas between surfaces are gaps.

cannot be accommodated on any structures directly in line with the anticlinal axis or its underlying backthrust.

Slip first appears on the backthrust defining the western limb of Horse Center anticline (Fig. 7, sections N–N′ and O–O′) immediately southeast of Cedar Mountain. Below the eastern limb of Horse Center anticline, seismic data show two NE-directed, basement-involved thrust faults that project northwestward into the approximate locations of the two Line Creek splays. Unfortunately, east and northeast of Horse Center Anticline, well and available seismic data are limited and/or restricted to the sedimentary cover rocks, leaving the 3D geometry of the intersection of the Line Creek and Horse Center footwalls and the Oregon Basin hanging wall unconstrained.

At the northern plunge of Oregon Basin anticline, formation top and dip data from five wells indicate a continuous, approximately 20° north-dipping monoclinal fold at the level of the Mississippian Madison Limestone. This monoclinal nose of the Oregon Basin anticline suggests that the Cedar Mountain tear fault does not cut the basement nonconformity within the Line Creek footwall, and that the Oregon Basin fault loses slip northward via distributed slip loss rather than at a discrete tear fault within the sedimentary strata. The geometry of northward slip loss on the Oregon Basin fault is similar to that observed in seismic data along the southward-terminating intermediate fault blocks of the Beartooth fault system. This transition also defines a large eastward step in the basin-boundary fault system from the Line Creek–Beartooth fault system to the Oregon Basin fault to the south.

This complex set of transitions suggests that detached cover strata and fault-bounded basement blocks moved independently. The Rattlesnake Mountain and Horse Center anticlines appear to terminate against a transverse fault zone located within the hanging wall of the Line Creek Fault system. Although this structure is not as regionally extensive as the right-lateral Tensleep Fault that crosses the southern Bighorn Basin (Hennings and Hager, 1996), the Cedar Mountain fault zone may have allowed partitioning and independent movement of basement blocks within the complexly-deformed hanging wall of the Line Creek fault system. This hypothesis may explain why backthrust structures like the Horse Center and Shoshone anticlines do not line up along-strike. Because the Cedar Mountain fault zone does not appear to extend eastward beyond the Line Creek fault system, the northward termination of the Oregon Basin fault in the approximate vicinity of this NE trend is more likely an eastward step in the deformation front via a north-dipping ramp, rather than a regionally-extensive strike-slip fault.

6. Discussion and conclusions

The transition from exposed basement thrusting in the Beartooth arch to blind thrusting on the Oregon Basin fault system shows that relatively simple, unidirectional Laramide stresses were complicated by the interplay of diverse fold mechanisms and pre-existing basement weaknesses. The complete dominance of thrust and strike-slip minor faulting indicating bed-parallel shortening confirms many recent studies (see summaries in Brown, 1993; Erslev, 2005) showing that horizontal compression was the dominant cause of Laramide basement-involved deformation. The lack of subsequent minor faults also shows that recent uplift related to the Yellowstone melting anomaly was not accompanied by significant internal deformation.

The uniformity of minor fault populations in this study area at locations away from anticlinal hinges indicates a single, sub-horizontal stage of shortening and compression. Minor faults in oblique folds show complex shortening directions, commonly multi-modal and differing from 065°, suggesting combinations of stress partitioning within folds and vertical axis rotations during oblique-slip deformation. Paleomagnetic investigations of vertical axis rotation in this area could help differentiate rotations from refraction and partitioning mechanisms.

The 2D cross-sections of the arch margin show a complicated array of fold geometries and kinematics. The largely-planar, rotated and minimally-distorted backlimb of Rattlesnake Mountain anticline suggests rotational fault-bend folding of a basement chip. The success of rotational basement block balancing (Erslev, 1986), whereby the basement is restored to a nearly continuous mosaic of blocks, confirms rotational fault-bend folding with minimal penetrative basement deformation in the Rattlesnake Mountain backlimb area. In contrast, penetrative inclined shear was needed to replicate the basement wedge geometries between the Rattlesnake Mountain footwall and hanging wall. The tighter, more symmetric Pat O'Hara Mountain anticline indicates a transpressional origin with substantial distributed basement deformation. Curved basement surfaces adjacent to the Line Creek fault system also indicate penetrative basement folding, perhaps while used as a hinge zone for backthrusting of the Rattlesnake Mountain anticline.

The degree of basement folding seems to be related to the presence of pre-existing weaknesses, whereby reactivation of pre-existing weaknesses produced little or no folding of basement rocks, and neo-formed basement faults caused basement to fold. In the case of Rattlesnake Mountain in Shoshone Canyon, the basement shows little evidence of folding, and map-scale faults parallel and include Precambrian dikes. Here, it appears that the fault propagated rapidly to the basement–cover interface along pre-existing dike contacts, causing little basement folding along the way. The penetrative shear that was modeled for the intermediate basement wedge of the Rattlesnake Mountain system may have resulted from accommodation of rigid-block rotation of the adjacent hanging wall or perhaps represents a component of slip unable to be accommodated by movement paralleling the pre-existing weaknesses.

The lack of clear penetrative basement folding and minor fault evidence of oblique-slip associated with the Beartooth and Pat O'Hara Mountain fault systems suggest that these faults also followed zones of basement weakness, like at Rattlesnake Mountain. In contrast, the Line Creek fault system opposite to Rattlesnake Mountain anticline shows basement folding, suggesting that the fault did not immediately break through the basement nonconformity but instead was preceded by basement-involved fault-propagation folding. This resistance to fault-propagation may have been the key reason why movement along this segment of the basin margin was shunted to the SW-directed Rattlesnake Mountain backthrust.

The structural geometry is further complicated within the sedimentary strata by backthrusts in the forelimbs of the major structures causing thin-skinned detachment and fault-propagation folding. In nearly every basement-involved fault, some of the slip was redirected up the steep limb of the fold, forming a triangle zone. This slip commonly resulted in "rabbit ear" structures where faults ramped out of bedding, forming thin-skinned, asymmetrical fault-propagation folds. Moreover, there may have been larger-scale, bedding-parallel decoupling and sliding into the basin during Laramide deformation.

The 3D geometries are similarly complex, showing both abrupt and gradual transitions on both regional and local scales. Regionally, the structural elevation of the Beartooth arch hanging wall remains high relative to the footwall along the western margin of the Bighorn Basin as the basin floor gradually drops southeastward to its lowest point, approximately 7 km below sea level, south of the Oregon Basin anticline. Along this margin, regional-scale abrupt changes are present in the form of jogs in arch trend at 1) the southward jog of the Beartooth arch at the MT/WY border and 2) the eastward step in the deformation front from the Line Creek to the Oregon Basin fault systems. At the local scale, the Line Creek relay-ramp represents a gradual transfer of slip between fault splays, whereas the transverse Cedar Mountain fault zone documents an abrupt transition from backthrusting at Rattlesnake Mountain anticline to fore-thrusting at Horse Center anticline.

Three-dimensional restoration of the southern Beartooth arch transition (Neely, 2006) shows that along-strike shortening is several percent less within the segment of the Line Creek fault system where backthrusting and basement folding of the hanging-wall tip are present. Local geometric complexities within arch transitions, including backthrusts, anticlinal intersections, basement wedges, and ramp structures appear to form due to a combination of lateral and vertical propagation of underlying basement faults that locally followed pre-existing structures. These structures can form within a uniformly-oriented shortening field, which locally may be complicated by oblique-slip, vertical axis rotations, and possibly fold-related stress re-orientation and strain partitioning. The continuous, yet sinuous nature of primary, basin-bounding fault systems and the diversity of geometric styles along-strike suggest that arch-bounding fault systems may form as networks of isolated faults, some neo-formed and others reactivated, which link during progressive arch development via lateral propagation.

Acknowledgments

This research was funded by grants from the Geological Society of America, the American Association of Petroleum Geologists, the Rocky Mountain Association of Geologists, the Wyoming Geological Association, the Colorado Scientific Society, Colorado State University/Edward Warner, and ConocoPhillips. 2DMove and 3DMove software were provided to Colorado State University by Midland Valley. Steve Bridges and Windsor Energy provided helpful discussion and access to several well and 2D and 3D seismic data sets. ConocoPhillips provided training in 3DMove software during a 2005 internship and access to an extensive 2D seismic data set that greatly improved the study. Particular thanks goes to Peter Hennings at ConocoPhillips for his scientific guidance, software training, and access to seismic data. Mark Fischer and Rick Groshong provided thoughtful and constructive reviews that contributed significantly to the structure and readability of the paper.

References

Allmendinger, R.W., Jordan, T.E., 1983. Andean tectonics related to geometry of subducted Nazca plate. Geological Society of America Bulletin 94, 341–361.
Allmendinger, R.W., 1998. Inverse and forward numerical modeling of trishear fault-propagation folds. Tectonics 17, 640–656.
Bird, P., 1998. Kinematic history of the Laramide Orogeny in latitudes 35 degrees-49 degrees N, western United States. Tectonics 17, 780–801.
Blackstone Jr., D.L., 1986. Structural geology – northwest flank of Bighorn Basin: Park County, Wyoming and Carbon County, Montana. In: Geology of the Beartooth Uplift and Adjacent Basins, Montana Geological Society and Yellowstone Bighorn Research Association Joint Field Conference and Symposium, pp. 125–135.
Bolay-Koenig, N.V., Erslev, E.A., 2003. Internal and external controls on Phanerozoic Rocky Mountain structures, USA: insights from GIS-enhanced tectonic maps. In: Raynolds, R.G., Flores, R.M. (Eds.), Cenozoic Systems of the Rocky Mountain Region: SEPM Rocky Mountain Section, pp. 33–63.
Brown, W.G., 1984. Rattlesnake Mountain anticline – a reverse fault interpretation. The Mountain Geologist 21, 32–35.
Brown, W.G., 1993. Structural style of Laramide basement-cored uplifts and associated folds. Wyoming Geology. University of Wyoming, Wyoming Geological Survey, pp. 313–371.
Chapin, C.E., Cather, S.M., 1981. Eocene tectonics and sedimentation in the Colorado Plateau-Rocky Mountain area. In: Dickinson, W.R., Payne, W.D. (Eds.), Relation of Tectonics to Ore Deposits in the Southern Cordillera. Arizona Geological Society Digest, vol. 14, pp. 173–198.
Clarey, T.L., 1990. Thin-skinned shortening geometries of the South Fork Fault: Bighorn Basin, Park County, Wyoming. The Mountain Geologist 27, 19–26.
Compton, R.R., 1966. Analyses of Pliocene–Pleistocene deformation and stresses in northern Santa Lucia Range, California. Geological Society of America Bulletin 77, 1361–1380.
DeCelles, P.G., Gray, M.B., Ridgway, K.D., Cole, R.B., Srivastava, P., Pequera, N., Pivnik, D.A., 1991. History and kinematics of foreland uplift from synorogenic conglomerate, Beartooth Range, Wyoming and Montana. Geological Society of America Bulletin 103, 1458–1476.
Durdella, M.J., 2001. Mechanical Modeling of Fault-related Folds: West Flank of the Bighorn Basin, Wyoming. M.S. Thesis, Purdue University.
Epard, J.L., Groshong, R.H., 1995. The role of strain in area-constant detachment folding. Tectonophysics 247, 85–103.
Erslev, E.A., 1986. Basement balancing of Rocky Mountain foreland uplifts. Geology 14, 259–262.
Erslev, E.A., 1990. Heterogeneous Laramide deformation in the Rattlesnake Mountain Anticline, Cody, Wyoming. In: Geologic Field Tours of Western Wyoming and Parts of adjacent Idaho, Montana, and Utah, Geological Survey of Wyoming, vol. 29 141–149.
Erslev, E.A., 1991. Trishear fault-propagation folding. Geology 19, 617–620.
Erslev, E.A., 1993. Thrusts, back-thrusts, and detachment of Laramide foreland arches. In: Schmidt, C.J., Chase, R., Erslev, E.A. (Eds.), Laramide Basement Deformation in the Rocky Mountain Foreland of the Western United States. Geological Society of America Special Paper, vol. 280, pp. 339–358.
Erslev, E.A., 2001. Multistage, multidirectional tertiary shortening and compression in north-central New Mexico. Geological Society of America Special Bulletin 113, 63–74.

Erslev, E.A., 2005. 2D Laramide geometries and kinematics of the Rocky Mountains, Western U.S.A. In: Karlstrom, K.E., Keller, G.E. (Eds.), The Rocky Mountain Region: An Evolving Lithosphere. Geophysical Monograph Series, vol. 154, pp. 7–20.

Erslev, E.A., Hennings, P.H., 2004. Variations in predicted reservoir heterogeneity due to multiple models of folding in basement-involved foreland anticlines. Abstracts with Programs, AAPG Annual Meeting.

Erslev, E.A., Larson, S.M., 2006. Testing Laramide hypotheses for the Colorado Front Range using minor faults. The Mountain Geologist 43, 45–64.

Gries, R.R., 1983. North-south compression of the Rocky Mountain foreland structures. In: Lowell, J.D., Gries, R.R. (Eds.), Rocky Mountain Foreland Basins and Uplifts. Rocky Mountain Association of Geologists, Denver, Colorado, pp. 9–32.

Hauge, T.A., 1993. The Heart Mountain detachment, northwestern Wyoming: 100 years of controversy. In: Snoke, A.W., Steidmann, J.R., Roberts, S.M. (Eds.), Geology of Wyoming: Geological Survey of Wyoming Memoir No. 5, pp. 530–571.

Hennings, P.H., Hager, 1996. Basement backthrusts and thin-skinned detachments in Goosebury Field, western Bighorn Basin, Wyoming, Wyoming Geological Association 47th Annual Field Conference Guidebook, pp. 221–238.

Humphreys, G., Hessler, E., Dueker, K., Farmer, L., Erslev, E., Atwater, T., 2003. How Laramide-aged hydration of the North American Lithosphere by the Farallon Slab controls subsequent activity in the western U.S. International Geology Review 45, 575–595.

Johnson, G.D., 1934. Geology of the mountain uplift transected by the Shoshone Canyon, Wyoming. Journal of Geology 42, 809–838.

Love, J.D., Christiansen, A.C., 1985. Geologic Map of Wyoming, USA. Geological Survey, Scale 1:500,000.

Marshak, S., Karlstrom, K.E., Timmons, J.M., 2000. Inversion of Proterozoic extensional faults: an explanation for the pattern of Laramide and Ancestral Rockies intracratonic deformation, United States. Geology 28, 735–738.

Neely, T.G., 2006. Three-Dimensional Strain at Foreland Arch Transitions: Structural Modeling of the Southern Beartooth Arch Transition Zone, Northwest Wyoming. M.S. Thesis, Colorado State University.

Petit, J.P., 1987. Criteria for the sense of movement on fault surfaces in brittle rocks. Journal of Structural Geology 9, 597–608.

Pierce, W.G., 1965a. Geologic map of the Clark Quadrangle, Park County, Wyoming. U.S. Geological Survey Geologic Quadrangle Map GQ-0477, Scale 1:62,500.

Pierce, W.G., 1965b. Geologic map of the Deep Lake Quadrangle, Park County, Wyoming. U.S. Geological Survey Geologic Quadrangle Map GQ-0478, Scale 1:62,500.

Pierce, W.G., 1966. Geologic map of the Cody quadrangle, Park County, Wyoming. U.S. Geological Survey Geologic Quadrangle Map GQ-542, Scale 1:62,500.

Pierce, W.G., 1970. Geologic map of the devils tooth quadrangle, Park County, Wyoming. U.S. Geological Survey Geologic Quadrangle Map GQ-817, Scale 1:62,500.

Pierce, W.G., Nelson, W.H., 1968. Geologic map of the Pat O'Hara Mountain Quadrangle, Park County, Wyoming. U.S. Geological Survey Geologic Quadrangle Map GQ-0755, Scale 1:62,500.

Pierce, W.G., Nelson, W.H., 1969. Geologic map of the Wapiti Quadrangle, Park County, Wyoming. U.S. Geological Survey Geologic Quadrangle Map GQ-0778, Scale 1:62,500.

Stearns, D.W., 1971. Mechanisms of drape folding in the Wyoming Province. 23rd Annual Field Conference Guidebook. In: Renfro, A.R. (Ed.), Symposium on Wyoming Tectonics and their Economic Significance. Wyoming Geological Association, pp. 125–143.

Stearns, D.W., 1975. Laramide basement deformation in the Bighorn Basin – the controlling factor for structure in the layered rocks. 27th Annual Field Conference Guidebook. Wyoming Geological Association, pp. 149–158.

Stearns III, D.W., 1978. Faulting and forced folding in the Rocky Mountain foreland. In: Mathews, V. (Ed.), Laramide Folding Associated with Block Faulting in the Western United States. Geological Society of America Memoir 151, pp. 1–37.

Stone, D.S., 1984. The Rattlesnake Mountain, Wyoming, debate: a review and critique of models. The Mountain Geologist 22, 37–46.

Stone, D.S., 1985. Geologic interpretation of seismic profiles, Bighorn Basin, Wyoming, Part II: West flank. In: Gries, R.R., Dyer, R.C. (Eds.), Seismic Exploration of the Rocky Mountain Region. Rocky Mountain Association of Geologists and Denver Geophysical Society Special Publication, pp. 175–186.

Suppe, J., 1983. Geometry and kinematics of fault-bend folding. American Journal of Science 283, 684–721.

Suppe, J., Medwedeff, D., 1990. Geometry and kinematics of fault-propagation folding. Eclogae Geologicae Helvetiae 83, 409–454.

Tikoff, B., Maxson, J., 2001. Lithospheric buckling of the Laramide foreland during Late Cretaceous to Paleogene, western United States. Rocky Mountain Geology 36, 13–35.

Varga, R.J., 1993. Rocky Mountain foreland uplifts: products of a rotating stress field or strain partitioning? Geology 21, 1115–1118.

Wise, D., 2000. Laramide structures in basement and cover of the Beartooth Uplift near Red Lodge, Montana. American Association of Petroleum Geologists Bulletin 84, 360–375.

Yu, G., 1993. Slip partitioning along major convergent plate boundaries. Pure and Applied Geophysics 140, 183–210.